

Retraction

Retracted: Modeling and Optimization of MRR in Wire Electrical Discharge Machining of Silicon Particle-Reinforced AA6063 Composite

Advances in Materials Science and Engineering

Received 26 December 2023; Accepted 26 December 2023; Published 29 December 2023

Copyright © 2023 Advances in Materials Science and Engineering. This is an open access article distributed under the Creative Commons Attribution License, which permits unrestricted use, distribution, and reproduction in any medium, provided the original work is properly cited.

This article has been retracted by Hindawi, as publisher, following an investigation undertaken by the publisher [1]. This investigation has uncovered evidence of systematic manipulation of the publication and peer-review process. We cannot, therefore, vouch for the reliability or integrity of this article.

Please note that this notice is intended solely to alert readers that the peer-review process of this article has been compromised.

Wiley and Hindawi regret that the usual quality checks did not identify these issues before publication and have since put additional measures in place to safeguard research integrity.

We wish to credit our Research Integrity and Research Publishing teams and anonymous and named external researchers and research integrity experts for contributing to this investigation.


The corresponding author, as the representative of all authors, has been given the opportunity to register their agreement or disagreement to this retraction. We have kept a record of any response received.

References

- [1] C. Mahesha, R. Suprabha, N. Bhavani et al., "Modeling and Optimization of MRR in Wire Electrical Discharge Machining of Silicon Particle-Reinforced AA6063 Composite," *Advances in Materials Science and Engineering*, vol. 2022, Article ID 2594974, 9 pages, 2022.

Research Article

Modeling and Optimization of MRR in Wire Electrical Discharge Machining of Silicon Particle-Reinforced AA6063 Composite

CR Mahesha,¹ R. Suprabha,¹ NPG Bhavani,² Prashant Sunagar,³ Raja Ramesh,⁴ P. Balamurugan,⁵ Rajasekar Rajendran,⁶ and Anirudh Bhowmick⁷ 

¹Department of Industrial Engineering & Management, Dr. Ambedkar Institute of Technology, Bangalore, Karnataka 560056, India

²Department of Electronics and Communication Engineering, Saveetha School of Engineering, Saveetha Institute of Medical and Technical Sciences, Chennai, Tamil Nadu 602105, India

³Civil Engineering Department, M S Ramaiah Institute of Technology, Bengaluru, Karnataka 560054, India

⁴Department of Mechanical Engineering, Sri Vasavi Institute of Engineering and Technology, Nandamuru, Andhra Pradesh 521369, India

⁵Department of Mathematics, M.Kumarasamy College of Engineering, Karur, Tamil Nadu 639113, India

⁶Department of Automobile Engineering, Bharath Institute of Higher Education and Research, Chennai, Tamil Nadu 600073, India

⁷Faculty of Meteorology and Hydrology, Arba Minch Water Technology Institute, Arba Minch University, Ethiopia

Correspondence should be addressed to Anirudh Bhowmick; anirudh.bhowmick@amu.edu.et

Received 19 March 2022; Accepted 30 May 2022; Published 30 June 2022

Academic Editor: Palanivel Velmurugan

Copyright © 2022 CR Mahesha et al. This is an open access article distributed under the Creative Commons Attribution License, which permits unrestricted use, distribution, and reproduction in any medium, provided the original work is properly cited.

Improved properties can be found in aluminum alloys containing silicon carbide reinforcement particles. This work studies the machinability of Al 6063 reinforced with silicon carbide particles with wire electrical discharge machining. To attain a high material removal rate, wire EDM constraints such as current (I), pulse-on time (T_{on}), wire speed (W_s), voltage (I_v), and pulse-off time (T_{off}) can be adjusted with precision. Taguchi L16 orthogonal arrays are used to design the experiments and statistical methods are used to examine. These process characteristics had a significant impact on the overall rate of return, with a 28.2% impact on the MRR, 23.04% impact on the MRR, and 22.86% impact on the MRR. We achieved MRRs of 65.21 mg/min for samples containing 5% and 10% SiCp at optimal conditions, respectively. Linear regression was used to create the statistical model, which then used confirmation trials to verify its accuracy in predicting MRR ($R^2 = 73.65\%$). The statistical model is used to estimate MRR based on various process parameter settings.

1. Introduction

Machining using EDM is an isolated phenomenon and removes material by repeatedly igniting a conductor and the workpiece in a dielectric liquid [1]. This fluid circulates to remove molten debris from the work area while it is being machined. You can use wire EDM to make complex forms out of conductive metals like aluminum, copper, brass, titanium, and other alloys [2]. While other technologies can produce thin walls with low surface roughness and short internal corner radii, wire EDM has the advantage of having

the least amount of burrs [3]. This approach's speed and economy are two additional perks. As a result of their low density, aluminum alloys are extensively employed in the transportation industry (aircraft, planes, and ships). Of the total, the transportation sector consumes 23%, followed by construction (25%), packing (8%) and engineering (11%), and electrical appliances (6%). This metal has a low density, high malleability, resistance to corrosion, and electrical conductivity [4, 5]. The aluminum 6000 series' superior mechanical and welding characteristics enable a wide range of goods, including aviation fittings and electrical

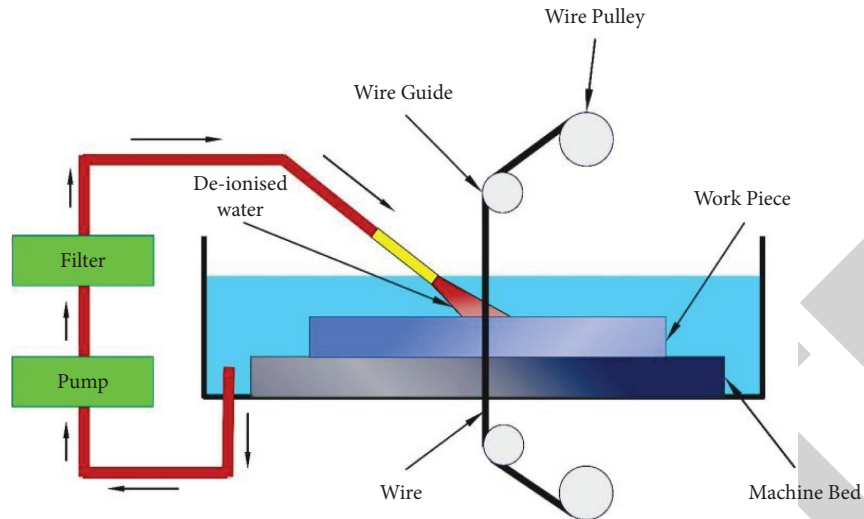


FIGURE 1: Schematic view of wire cut electrical discharge machine.

components and connections, camera lens mounting, and marine fits and accessories.

Alloying it with other substances like silicon carbide (SiC), aluminum oxide (Al_2O_3), magnesium oxide (MgO), water-glass (WC), silicon dioxide (SiO_2), or boron carbide (B_4C), etc, the inclusion of SiC and Al_2O_3 particles in an aluminum matrix enhanced yield strength (YS), ultimate tensile strength (UTS), elastic modulus (EM), and hardness (Hd), according to [6]'s research. Electrical conductivity was reduced by the addition of aluminum oxide, zirconium, cerium, and Mg. In comparison to the as-cast alloy, the age-hardened Al 6063-SiCp-reinforced composites demonstrated an increase in hardness of 120–145% [7]. Compared to high-temperature aging, lower-temperature aging demonstrated a significant improvement in wear resistance. Size reduction was achieved with the inclusion of grain refiners (Al-5Ti-1B), which also turned a long, coarse grain into a circular one with improved tensile and wear resistance. Strength/weight ratio, superior thermal stabilization, and abrasive resistance make SiCp a useful reinforcing particle [8, 9]. Al 6063 with SiCp had enhanced Young's modulus, strength, and toughness (500 nm). An investigation of Al MMC strengthened with silicon and Tungsten carbide was conducted by [10]. Load is transferred to the reinforcement through the robust interface among the matrix and strengthened composites. This procedure enhanced both elasticity and strength. References [11, 12] used continuous mechanical simulations to show that whiskers of Tungsten carbide and aluminum nitride strengthen Al composites. Figure 1 shows the schematic view of the wire cut electrical discharge machine.

The abrasive character of SiCp-reinforced aluminum alloys makes machining them challenging, which results in rapid tool wear and a poor surface finish [13]. Particle detachment and fracture in reinforced particles are what cause voids and cavities on the machined surface to appear. Nontraditional methods such as wire EDM (electrical discharge generated between the tool and workpiece) may be an option for removing metal from the workpiece [14, 15]. The

base metal is molten and vaporized by the spark gap's concentrated heat. The spark gap is filled with dielectric fluid, which is used to cool the machine as well as control the discharge of electricity. This procedure has a drawback in that it requires a workpiece that is electrically conducting [16–19]. Among the benefits of wire EDM are its ability to produce complicated profiles regardless of the workpiece's mechanical qualities and the fact that tools and workpieces do not come into direct touch during the machining process. Currently, wire EDM research trends are mostly focused on scientific research of application areas and optimization of processing variables [20]. For vehicle nozzles, turbine blade cooling holes, medicinal devices such as stents, microfluidic channels, and the fabrication of different micro-electromechanical devices, EDM has become increasingly popular in recent years. Polishing 3D printed parts with the wire EDM reduces surface roughness by roughly 80%, making it a useful tool for other applications as well [21]. The eradication of balling pits, voids, and porosity could be seen in the 3D printed SS316L material that had been polished with wire EDM. Because the long discharge time of the high ton produced roughness, the wire EDM polishing application of the low ton was promoted. Electrode wires are visible on the polished surface, accumulating in extremely small amounts [22].

Once it came to aluminum composites, [23] studied the effects of hot extrusion and heated treatment on reinforced SiCp size (0.7–13 μm). Smaller-sized SiCp and 0% particles were not significantly different in the surface quality after wire EDM. Both the kerf breadth and the electrode wear on the smaller-sized SiCp were greater than on test samples reinforced with larger particles [24, 25]. Moreover, the wire electrode was coated with matrix material during the milling process. Mixing MWCNTs into the dielectric fluid resulted in an increase in machining performance. Shape memory alloy nitinol wire EDM treated with MWCNTs (1 g/L) showed a 75.42% increase in MRR and a 19.15% decrease in SR. Additionally, it was determined that the recast layer's thickness

TABLE 1: Composition (%) of Al 6063.

Silicon	Iron	Copper	Magnesium	Manganese	Others	Aluminum
0.41	0.11	0.05	0.49	0.1	0.05	Remaining

had decreased significantly. Al413 - 9% composite was studied by [26] for its wire EDM machinability. The kerf-width and surface roughness were highly correlated with the machine's voltage, capacitance, and feed rate. Improving the supply enhanced the MRR during SiC/Al composite machining. Matrix SiCp content increases by 15%, whereas subsequent increases in SiC content increase the MRR in the opposite way [27]. The AA6025 composite was tested for its surface coarseness and material removal rate (silicon carbide: 10 wt% and aluminum oxide:10 wt.%) [28]. The conductive powder was shown to improve performance in the dielectric fluid by the researchers, according to their findings. This is because the conductive particles have diminished the dielectric fluid's strength and hence increased the spark gap. As a result of this phenomenon, the spark gap discharge remained more stable and higher during the ignition process. Researchers of [29, 30] used a 6%SiC/A356 surface to better understand EDM surface features. SiC/A359 is 30% and 10% SiC/Al359 is 30%. The harder the surface became, the denser the reinforced particles became. In EDM, copper electrodes transport a lot more metal than graphite electrodes. Researchers of [31–33] enhanced the wire EDM parameter settings to machine an Al 6063/cenosphere composite. In addition to increasing in size, the craters' surface wave smoothness also increased as I and T_{on} . Electrode wear is increased because of the composite's poor surface quality.

The weight percentage and volume percentage of reinforcing particles in the matrix influence the composite's mechanical properties. When reinforcing particles are consistently distributed throughout the material, the mechanical characteristics of composites improve [34]. Due to increased stress, reinforcing materials began forming aggregates that reduced their mechanical qualities. SiCp up to 10% was shown to boost tensile and hardness; however, after that point, these properties rapidly deteriorated. However, ductility decreased as the amount of SiCp in the alloy rose. More than 8% SiCp loading resulted in aggregated particles in the Al 6063 matrix when stir casting was performed on test samples. As a result, in this project, the weight fraction is capped at 8%. Traditional machining of Al-SiCp is plagued by pits, voids, microcracks, and cracked reinforcements on the cut surface. Wire EDM machining, for example, can get around these problems [35]. Wire EDM process constraints including T_{on} and T_{off} , W_s , and I_v are examined in this analysis in order to optimize these settings in order to maximize productivity in terms of the MRR. Fuzzy AHP-ARAS, genetic algorithms, and particle swarm optimization methods like the Grass-Hopper method and moth-flame are more appealing for experiments with large data sets; however, Taguchi and response surface approaches, as used in this study, are better instruments for optimization in small-scale experiments [36]. As a result, the Taguchi technique is used in this study to

TABLE 2: Wire electrical discharge machining process parameters and factors.

Factors	Code	1	2	3	4
I (A)	A	4	5	6	7
T_{on} (μ s)	B	25	35	45	55
T_{off} (μ s)	C	15	20	25	30
W_s (rpm)	D	180	360	720	1440
I_v (V)	E	90	100	-	-

optimize the MRR and build a regression model that reliably predicts the MRR.

2. Materials and Methods

Sample preparation, experimental setup, wire EDM processing parameters, and design of experiments are all covered in this part. The response parameter and optimization approach are also discussed.

2.1. Details of the Experiment and the Specimens. In this study, researchers in India employed a CNC 2-axis wire EDM manufactured by accord wire EDM. Mo wire with a width of 0.16 mm is employed to make the tool electrode. Soft water and gel make up the insulator. The regulator has a 0.001 mm resolution. Stir casting is employed to create the SiC particle-reinforced Al-6063 alloy. By mechanically stirring the molten metal, reinforcing particles (5 and 10% by weight) that have been preheated to 650°C are evenly distributed throughout the molten matrix, which is liquefied at 850°C. The molten metal is poured into a mold that has been preheated to 200 °C and allowed to cool to room temperature before being moved. Table 1 provides an overview of the Al 6063 composite's chemical makeup.

2.2. Design of Experiments. There is a numeral factor that affects the MRR of a wire EDM system including current and pulse duration, wire speed, and voltage. Variations in voltage and other parameters are made at two separate levels. Detailed parameters and factors for the wire EDM technique may be found in Table 2. Based on the results of the tests, these levels have been chosen. The L16 Taguchi orthogonal array is chosen since the experiments require a total of 13 degrees of freedom. Table 3 outlines the experiment's plan of action. There was a total of two experiments per condition. The thickness of the specimens and the dielectric fluid supply pressure remained persistent during the processing.

2.3. Dimension of Material Removal Rate. For a total of 20 mm, test specimens are put through wire EDM according to the procedure outlined in Table 2. (1) calculates MRR based on weight loss during machining for each experimental session. Digital mass stability is employed to determine the

TABLE 3: Design of Experiments and associated mean material removal rate.

Trial no.	Process parameters settings				Material removal rate		
	I	t_{on}	t_{off}	W_s	V	5%	10%
1	4	25	15	1440	90	0.382	0.315
2	4	35	20	720	90	0.412	0.402
3	4	45	25	360	100	0.375	0.376
4	4	55	30	180	100	0.198	0.196
5	5	25	20	360	100	0.495	0.484
6	5	35	15	180	100	0.456	0.442
7	5	45	30	1440	90	0.521	0.496
8	5	55	25	720	90	0.416	0.404
9	6	25	25	180	90	0.258	0.235
10	6	35	30	360	90	0.324	0.318
11	6	45	15	720	100	1.176	1.126
12	6	55	20	1440	100	1.019	0.945
13	7	25	30	720	100	0.712	0.622
14	7	35	25	1440	100	0.546	0.527
15	7	45	20	180	90	0.863	0.664
16	7	55	15	360	90	0.742	0.723

weightage of specimens before and after machining (w_i and w_f) (accuracy: 0.001 g). Five measurements were done for each sample to assure accuracy. The mean MRR of each testing for each sample with varying SiCp compositions is shown in Table 3. Figure 2 depicts cut surfaces of test materials machined under various circumstances.

$$MRR = \frac{w_i - w_f}{t} \text{ mg/s.} \quad (1)$$

2.4. Optimization of Material Removal Rate. An ANOVA technique was used to analyze wire EDM properties such as I , T_{on} and T_{off} , W_s , and V to assess their influence on material removal rate. With a 95% degree of confidence, the F-test is used to identify important process parameters. It is also possible to calculate the average MRR at several levels (Levels). The best conditions for a high MRR are determined for each of the study's process parameters based on the MRR levels that yield the highest MRR. Equations (2)–(5) are used to calculate the MRR under optimal conditions. Finally, regression analysis is used to construct a statistical model that can predict the MRR using regression coefficients.

$$n_{eff} = \frac{n}{1 + DF} \quad (2)$$

$$T = \frac{\sum MRR}{n} \quad (3)$$

$$MRR_{Optimum} = MRR[A_3 B_3 C_1 D_3 E_2] - 4 \times T, \quad (4)$$

$$\text{Confidence interval} = \pm \sqrt{F(\alpha, DF_{error}) \times \frac{MS_{error}}{n_{eff}}}. \quad (5)$$

2.5. Material Removal Theoretical Modeling. In wire EDM, the material is removed by a spark gap electric discharge. The

amount of spark energy generated through the sparking processing is calculated using (6). The quantity of heat generated by a spark is dependent on the spark's I , T_{on} , and I_v . Researchers employ the Gaussian heat input model to forecast the r_{sp} , despite the fact that other models exist. The axis of a spark has the highest heat intensity (qR) according to this model, and the heat flux related to this is represented by formula (7). The electric field among the electrode and workpiece ionizes the dielectric liquid, allowing electrons to flow freely. Eventually, a spark forms, which is hot enough to melt and evaporate the workpiece. The equation can be used to calculate the size of hemisphere craters created on the machined surface as an outcome of this phenomenon (8).

$$E_s = I_p \times I_v \times t_{on}, \quad (6)$$

$$q_f(R) = \frac{4.45 \times W_M \times I \times V}{\Pi \times (r_{sp})^2} \times e^{-4.5(R/r_{sp})^2}, \quad (7)$$

$$\Gamma = \frac{2}{3} \pi r^3. \quad (8)$$

3. Results and Discussion

3.1. Current and Wire Speed Have an Effect on MRR. As seen in Figure 2(a), MRR is influenced by the current. From 4 A to 6 A, the MRR rises significantly. At a current of 5 A, the highest material removal rate is 0.662 mg/s. The breakdown voltage and spark energy rise as the current increases from low to high values, as seen in (6). The high current melts and evaporates more material because of the higher. Other scholars have also found similar patterns. However, the MRR decreased slightly when the current was greater than 5 A. When there is not enough flushing from the molten pool, the recast layer forms on top of previously machined surfaces. During a discharge, debris dissolves from the dielectric fluid and degraded wire electrode particles are deposited as

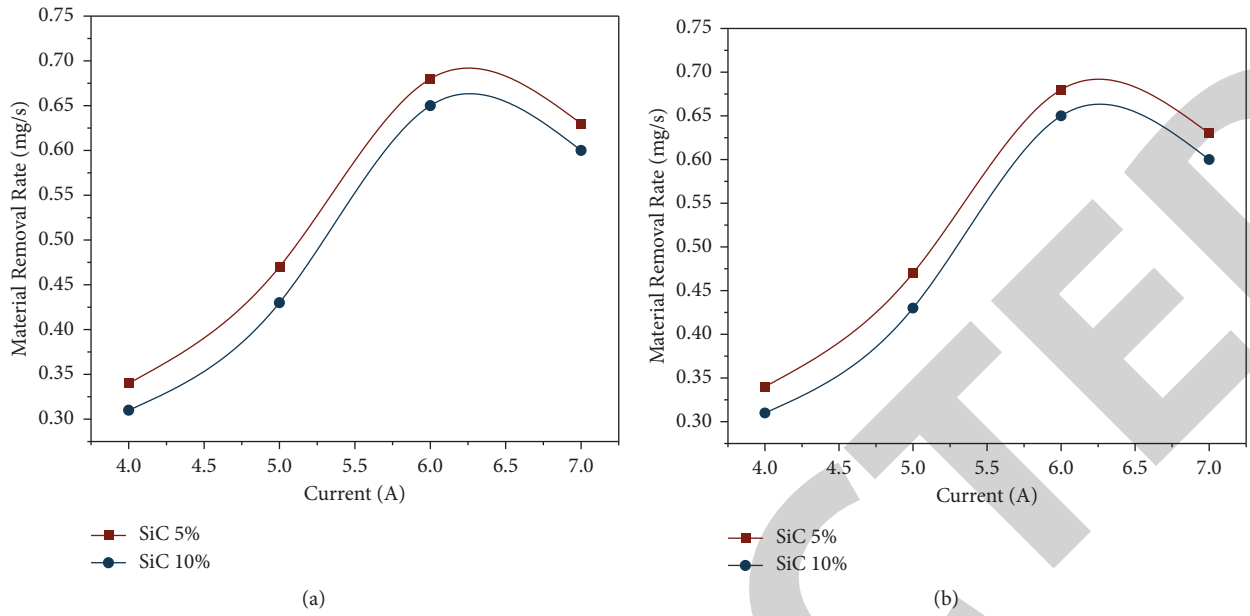


FIGURE 2: (a) Impact of I on material removal rate. (b) Impact of W_s on MRR.

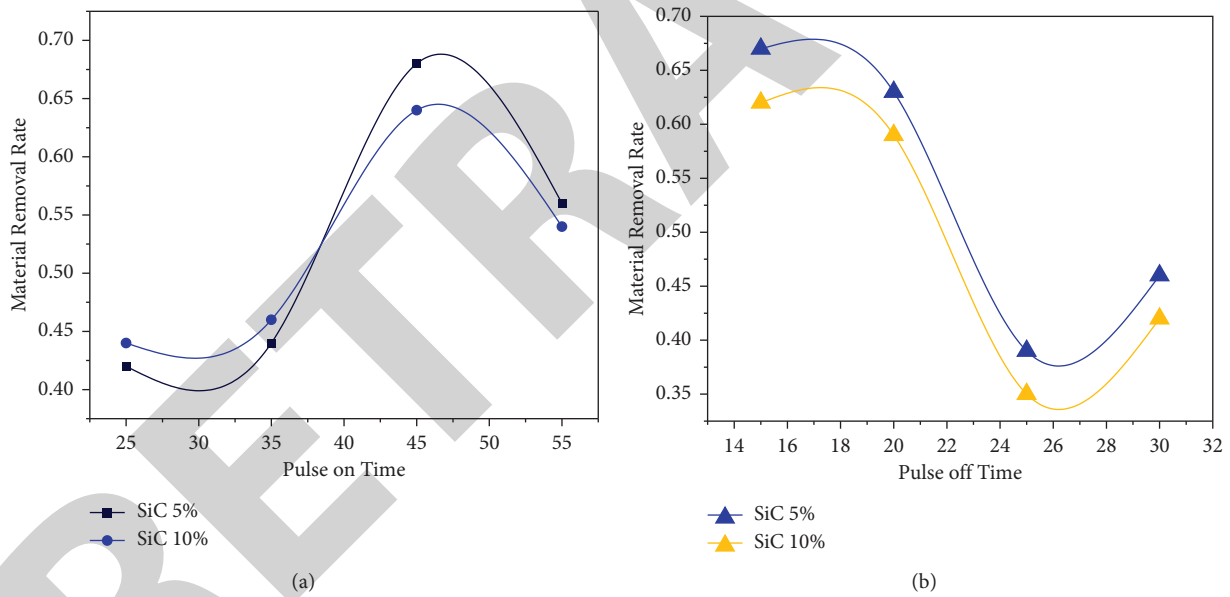


FIGURE 3: (a) Impact of t_{on} on material removal rate. (b) Impact of t_{off} on material removal rate.

the discharge energy increases to its maximum value. When current parameters are exceeded, the quick deposition of wreckage at the machining gap has a substantial effect on dielectric breakdown characteristics and material removal rate. As indicated in the image, wire speed has an impact on MRR, as illustrated in Figure 2(b). When the spool around which the electrode wire is coiled has a rotating speed of 180 to 1440 revolutions per minute, the MRR is indicated in Figure 2(b). The material removal rate rises from 0.382 mg/s to 0.664 mg/s when the spool rotation speed increases up to 720 revolutions per minute. When the spool's rotational speed was increased even further, the MRR was reduced by 10.52%. This is owing to the fact that when wire speed

increases, the quantity of spark energy obtainable for machining declines. Because of this, as wire speeds increase, the MRR falls.

3.2. *The Impact of Pulse-On Time (T_{on}) and Pulse-Off Time (T_{off}) on MRR.* MRR is affected by T_{on} and T_{off} times in Figure 3(a) and Figure 3(b). From 25 to 45s pulse-on time, the MRR was improved. Each spark's energy (E) is equal to $E = VI T_{on}$. As a result, larger craters are formed as a result of a longer pulse-on period. However, the MRR decreased from 0.685 mg/s to 0.582 mg/s when the pulse-on time exceeded 45 s. Longer cycles and lower spark frequencies, as shown in

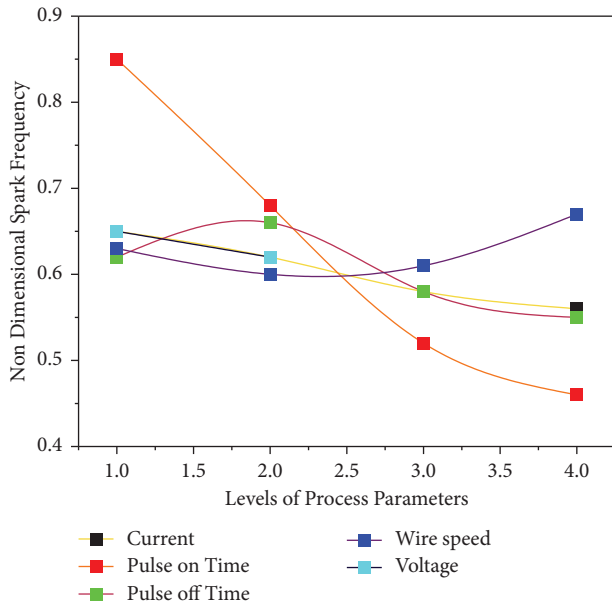


FIGURE 4: Spark frequency at variant levels.

Figure, may have resulted in the reforming of the molten pool surrounding the craters.

A consistent drop in MRR was seen as a result of increasing the pulse-off period from 15 seconds to 30 seconds, as depicted in Figure 4. During the pulse-off period, there is no sparking. As illustrated in Figure 4, growing the pulse time lengthens the cycle while decreasing the spark frequency. The MRR decreased as pulse-off time increased.

3.3. The Impact of Voltage on Material Removal Rate. The impact voltage on material removal rate is shown in Figure 5. MRR appears to be directly influenced by voltage. The MRR rises by 24.45% while the spark gap voltage rises from 90 V to 100 V. V , I , and T_{on} all affect the spark energy ($E = V I t_{on}$), as previously stated. As a result of the increased voltage, a larger volume of material was melted and vaporized, raising the MRR.

As an outcome of the electrical spark among the wire electrode and the substance, the dielectric fluid experiences an abrupt rise in pressure. The holes on the machined surface appear because of the increasing pressure on the molten pool. There are also a few globules of partly molten metal on the machined surfaces.

A few of the SiCp particles may be found on the cut surface of the cast layer, showing that they were relocated during the cutting process. This is because dielectric fluid is circulated during the machining process. To collect the heated reinforced molten particles, dielectric fluid is pumped over the machining surface. As the molten matrix pool hardens, these particles are fused to the machined surface. The majority of the crater looks to have a truncated sphere shape based on these photographs. Using a Gaussian heat distribution model, the predicted spark radius is in agreement with this result. There is an extended feature on the machined surface near the crater boundaries. There is a piece

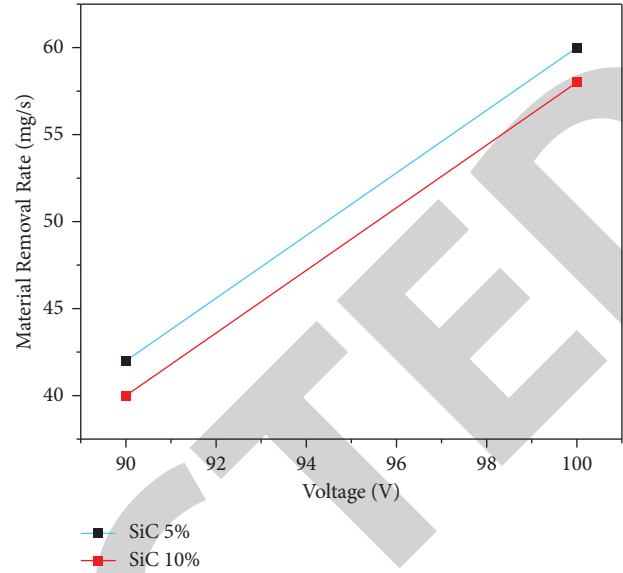


FIGURE 5: The impact voltage on material removal rate.

TABLE 4: ANOVA for material removal rate.

Source	Df	5% SiC			10% SiC		
		Seq SS	Adj MS	F	Seq SS	Adj MS	F
I	3	0.3140	0.1211	58.2	0.3156	0.1052	51.9
T_{on}	3	0.1862	0.0582	34.16	0.1862	0.0724	30.4
T_{off}	3	0.2416	0.0785	45.41	0.2621	0.08512	41.6
W_s	3	0.1440	0.0482	27.23	0.1543	0.0508	25.8
V	2	0.0812	0.0812	47.5	0.0856	0.0856	41.8
Residual error	2	0.0036	0.0019		0.3244	0.114	-
Total	16	0.9412	-	-	-	-	-

of the particle encased in the matrix material, making it more difficult to extract the reinforced SiCp. The spark gap exposes the remaining protruding portion to high temperatures. Sparks and traveling wire electrodes both have a significant impact on reinforced particles, causing shock waves and a mechanical moment. All the SiCp particles remain attached to the machined surface, and there is no evidence of debonding from the matrix. The quick cooling of molten metal and the segregation of alloying elements Mg, Si, etc. are largely responsible for the existence of blow holes. Blow holes are formed on a machined surface by a sparking process in the dielectric medium.

3.4. ANOVA of Material Removal Rate. Table 4 displays the outcomes of the Analysis of Variance for the MRR. Process characteristics that significantly affect MRR can be found utilizing the F-test on the Analysis of Variance data with a 95% confidence level. They have a considerable impact on MRR since their F-values are above critical values for the above variables. The percentage of each process parameter's contribution is also taken into consideration. Among the several factors influencing the rate of material removal, current accounted for the largest

TABLE 5: The mean material removal rate.

Level	I	T _{on}	T _{off}	W _s	V
5% SiC _p					
1	0.324	0.423	0.669	0.579	0.452
2	0.465	0.428	0.632	0.652	0.597
3	0.676	0.679	0.392	0.481	-
4	0.649	0.572	0.412	0.392	-
Delta	0.352	0.264	0.284	0.259	0.152
10% SiC _p					
1	0.322	0.412	0.652	0.385	0.441
2	0.456	0.419	0.619	0.472	0.582
3	0.652	0.662	0.382	0.631	-
4	0.639	0.531	0.416	0.561	-
Delta	0.341	0.251	0.267	0.251	0.152

TABLE 6: The predicted and experimental material removal rate (mg/min) at optimal conditions.

Trial No	5%			10%		
	Predicted MRR	Experimental MRR	Error (%)	Predicted MRR	Experimental MRR	Error (%)
1	71.4	68.4	5.80	68.3	63.4	7.12
2	71.3	67.3	6.70	68.4	62.6	8.01
3	71.4	67.5	4.60	68.4	64.8	6.21
4	71.4	67.4	7.0	68.4	62.4	8.15

share (28.2%), tracked by V (23.04%), T_{off} (22.84%), T_{on} (16.12%), and W_s (13.02%).

3.5. Optimum of Process Parameters. When using wire EDM to machine Al 6063-SiCp composite, the Taguchi approach is used to optimize machining parameters for maximum MRR. Table 5 displays the average MRR based on various process parameter configurations. There is a maximum MRR at settings A₃B₃C₁D₂E₂, i.e., I at level 3 (6 A), T_{on} at level 3 (45 s), T_{off} at level 1, W_s set to the level of 3, and voltage set to 100 V, as shown in the following table (level 2). For samples containing 5% and 10% SiCp, the anticipated MRR is 68.23 mg/min and 68.16 mg/min, respectively. Table 6 displays the findings of the confirmation trials, which were also carried out. Experiments have shown that MRR is consistent with the model's predictions. This table also shows the greatest change (delta) in MRR resulting from changes in the settings of a variety of processes. The processing factors are sorted in terms of current impact based on delta values: I, II, III, IV, and V are the pulse-off and pulse-on times, as well as the wire speed.

3.6. Regression Modeling of Material Removal Rate. In this area, we will go through the specifics of creating a statistical model that can be used to estimate MRR based on a variety of process parameter values. I, T_{on}, T_{off}, w_s, I_v, and the material removal rate are established by using a statistical model. The modeling takes into account the primary impact of these variables. As shown in (9), the regression model generated for samples with 5% and 10% SiCp can be expressed as (10). The equation has a 73.6% coefficient of determination (R²).

$$y = c + k_1 \times x_1 + k_2 \times x_2 + \dots + k_n \times x_n, \quad (9)$$

$$\begin{aligned} \text{Material Removal Rate} = & -1.20 + 0.114 \times I + 0.00685 \\ & \times t_{on} - 0.0194 \times t_{off} + 0.000135 \\ & \times w_s + 0.0142 \times I_v. \end{aligned} \quad (10)$$

The accurateness of forecasting material removal rate by regression model is evaluated by directing confirmation experiments up to the limits of operating factors, that is, $4 \leq I \leq 7$; $25 \leq t_{on} \leq 55$; $15 \leq t_{off} \leq 30$; $380 \leq w_s \leq 1440$; $90 \leq I_v \leq 100$. Test samples with a 5% and a 10% MRR have been found to have similar actual MRR values. There is a 4.45% minimal and a mean prediction error material removal rate, respectively. 2.19 standard deviations from the mean indicate a significant deviation. Table 6 depicts the predicted and experimental material removal rate (mg/min) at optimal conditions.

4. Conclusions

This analysis examined the impact of factors including I, t_{on}, t_{off}, w_s, I_v on processing of 5 wt% to 10 wt% SiC_p – Al 6063 alloys by wire electrical discharge machining. It is possible to increase the productivity of wire EDM companies by using the optimal settings to increase the MRR when working with these composites. Results have led to the following conclusions.

- (i) MRR was significantly influenced and rose by current, pulse-on time, pulse-off time, wire speed, and voltage but declined with rising pulse-off time and also wire speed over 720 rpm.

- (ii) The voltage (23.04%), pulse-on time (22.86%), pulse-off time (16.12%), and wire speed all contributed to MRR fluctuation to a lesser extent than the current (28.2%) wire speed (13.04%).
- (iii) The optimal setup which formed the greatest material removal rate (66.32 mg/min and 62.41mg/min for samples with 5% and 10% SiC_p) is current –6A, Pulse on time – 45 μ s, Pulse off time – 15 μ s, wire speed – 720rpm, and voltage-100 V.
- (iv) It is possible to estimate the MRR in wire EDM of Al 6063 with SiC, -p. up to 10 wt% within the operational range using the statistical model (mean, R²-73.65%).
($4A \leq I \leq 7A$; $25\mu s \leq t_{on} \leq 55\mu s$; $15\mu s \leq t_{off} \leq 30\mu s$; $380rpm \leq w_s \leq 1440rpm$; $90V \leq I_v \leq 100V$). The proposed regression model's MRR prediction error ranges from 4.45% to 20.46%.

Data Availability

The data used to support the findings of this study are included within the article. Further data or information are available from the corresponding author upon request.

Conflicts of Interest

The authors declare that there are no conflicts of interest regarding the publication of this paper.

Acknowledgments

The authors appreciate the support from Arba Minch University, Ethiopia, for the research and preparation of the manuscript. The authors thank Dr. Ambedkar Institute of Technology, M. S. Ramaiah Institute of Technology, and Sri Vasavi Institute of Engineering and Technology for providing assistance to complete this experimental work.

References

- [1] R. Ramesh, S. Suresh Kumar, D. Purushothaman, and N. T. Jeeva, "Performance study on copper coated tool using powder mixed EDM of monel 400," *Applied Mechanics and Materials*, vol. 766-767, pp. 600–605, 2015.
- [2] A. Perumal, C. Kailasanathan, B. Stalin et al., "Multiresponse optimization of wire electrical discharge machining parameters for Ti-6Al-2Sn-4Zr-2Mo (α - β) alloy using taguchi-grey relational approach," *Advances in Materials Science and Engineering*, vol. 2022, Article ID 690523, 13 pages, 2022.
- [3] M. A. Rahman, A. Ahmed, and M. Mia, "Trends in electrical discharge machining of Ti- and Ni-based superalloys: macro-micro-compound arc/spark/melt process," *Micro Electro-Fabrication*, Elsevier, vol. 2021, pp. 63–87, 2021.
- [4] J. Boban, A. Ahmed, M. A. Rahman, and M. Rahman, "Wire electrical discharge polishing of additive manufactured metallic components," *Procedia CIRP*, vol. 87, pp. 321–326, 2020.
- [5] V. Mohanavel and M. Ravichandran, "Influence of AlN particles on microstructure, mechanical and tribological behaviour in AA6351 aluminum alloy," *Materials Research Express*, vol. 6, no. 10, Article ID 1065, 2019.
- [6] R. Chaudhari, S. Khanna, J. Vora et al., "Experimental investigations and optimization of MWCNTs-mixed WEDM process parameters of nitinol shape memory alloy," *Journal of Materials Research and Technology*, vol. 15, pp. 2152–2169, 2021.
- [7] P. Sivaprakasam, P. Hariharan, and S. Gowri, "Optimization of micro-WEDM process of aluminum matrix composite (A413-B4C): a response surface approach," *Materials and Manufacturing Processes*, vol. 28, no. 12, pp. 1340–1347, 2013.
- [8] H. Hocheng, W. T. Lei, and H. S. Hsu, "Preliminary study of material removal in electrical-discharge machining of SiC/Al," *Journal of Materials Processing Technology*, vol. 63, no. 1–3, pp. 813–818, 1997.
- [9] B. Singh, J. Kumar, and S. Kumar, "Influences of process parameters on MRR improvement in simple and powder-mixed EDM of AA6061/10% SiC composite," *Materials and Manufacturing Processes*, vol. 30, no. 3, pp. 303–312, 2015.
- [10] A. Kumar Sharma, R. Bhandari, A. Aherwar, and C. Pinca-Bretotean, "A study of fabrication methods of aluminum based composites focused on stir casting process," *Materials Today Proceedings*, vol. 27, pp. 1608–1612, 2020.
- [11] V. Mohanavel, S. Suresh Kumar, V. Sivaraman, V. K. Girish, and M. Ravichandran, "Tungsten carbide particulate reinforced AA7050 aluminum alloy composites fabricated by liquid state processing," *AIP Conference Proceedings*, vol. 2283, Article ID 020087, 2020.
- [12] M. Ravichandran, V. Mohanavel, T. Sathish, P. Ganeshan, S. Suresh Kumar, and S. Ram, "Mechanical properties of AlN and molybdenum disulfide reinforced aluminium alloy matrix composites," *Journal of Physics: Conf. Ser.*, vol. 2027, Article ID 012010, 9 pages, 2021.
- [13] P. N. Singh, K. Raghukandan, M. Rathinasabapathi, and B. C. Pai, "Electric discharge machining of Al-10% SiCP as-cast metal matrix composites," *Journal of Materials Processing Technology*, vol. 155, pp. 1653–1657, 2004.
- [14] S. S. Habib, "Study of the parameters in electrical discharge machining through response surface methodology approach," *Applied Mathematical Modelling*, vol. 33, no. 12, pp. 4397–4407, 2009.
- [15] S. S. Agrawal and V. Yadava, "Modeling and prediction of material removal rate and surface roughness in surface-electrical discharge diamond grinding process of metal matrix composites," *Materials and Manufacturing Processes*, vol. 28, no. 4, pp. 381–389, 2013.
- [16] S. Singh and A. Bhardwaj, "Review to EDM by using water and powder-mixed dielectric fluid," *Journal of Minerals and Materials Characterization and Engineering*, vol. 10, no. 2, pp. 199–230, 2011.
- [17] S. S. Sidhu, A. Batish, and S. Kumar, "Study of surface properties in particulate-reinforced metal matrix composites (MMCs) using powder-mixed electrical discharge machining (EDM)," *Materials and Manufacturing Processes*, vol. 29, no. 1, pp. 46–52, 2014.
- [18] A. Dey, S. Debnath, and K. M. Pandey, "Optimization of electrical discharge machining process parameters for Al6061/cenosphere composite using grey-based hybrid approach," *Transactions of Nonferrous Metals Society of China*, vol. 27, no. 5, pp. 998–1010, 2017.
- [19] S. S. Kumar, M. Uthayakumar, S. T. Kumaran, and P. Parameswaran, "Electrical discharge machining of Al (6351)-SiC-B4C hybrid composite," *Materials and Manufacturing Processes*, vol. 29, no. 11–12, pp. 1395–1400, 2014.

- [20] H. K. Issa, A. Taherizadeh, A. Maleki, and A. Ghaei, "Development of an aluminum/amorphous nano-SiO₂ composite using powder metallurgy and hot extrusion processes," *Ceramics International*, vol. 43, no. 17, pp. 14582–14592, 2017.
- [21] M. Ravikumar, H. N. Reddappa, and R. Suresh, "Aluminium composites fabrication technique and effect of improvement in their mechanical properties - a review," *Materials Today Proceedings*, vol. 5, no. 11, pp. 23796–23805, 2018.
- [22] I. M. El-Galy, M. H. Ahmed, and B. I. Bassiouny, "Characterization of functionally graded Al-SiC p metal matrix composites manufactured by centrifugal casting," *Alexandria Engineering Journal*, vol. 56, no. 4, pp. 371–381, 2017.
- [23] G. Shankar, S. S. Sharma, A. Kini, S. Praksh, and G. Gurumurthy, "Influence of artificial aging on the stir cast Al6061-SiC metal matrix composites under different aging conditions," *International Journal of Technology*, vol. 7, no. 6, pp. 1000–1008, 2016.
- [24] B. Sen, S. A. I. Hussain, A. Das Gupta, M. K. Gupta, D. Y. Pimenov, and T. Mikołajczyk, "Application of type-2 fuzzy AHP-ARAS for selecting optimal WEDM parameters," *Metals*, vol. 11, no. 1, p. 42, 2021.
- [25] A. Abbas, D. Pimenov, I. Erdakov, M. Taha, M. El Rayes, and M. Soliman, "Artificial intelligence monitoring of hardening methods and cutting conditions and their effects on surface roughness, performance, and finish turning costs of solid-state recycled aluminum alloy 6061 ?" *Metals*, vol. 8, no. 6, p. 394, 2018.
- [26] D. Dhaneswara, R. N. Verdiyanto, and A. Z. Syahrial, "The mechanical properties of Al₂O₃-reinforced aluminum A356 with grain refiner Al-5Ti-1B fabricated using the stir casting method," *International Journal of Technology*, vol. 8, no. 8, pp. 1489–1497, 2017.
- [27] N. Lenin, M. Sivakumar, G. Selvakumar et al., "Optimization of process control parameters for wedm of Al-LM25/Fly ash/B4C hybrid composites using evolutionary algorithms: a comparative study," *Metals*, vol. 11, no. 7, p. 1105, 2021.
- [28] J. Gu, Z. Lv, Y. Wu, R. Zhao, L. Tian, and Q. Zhang, "Enhanced thermal conductivity of SiCp/PS composites by electrospinning-hot press technique," *Composites Part A: Applied Science and Manufacturing*, vol. 79, pp. 8–13, 2015.
- [29] J. Gu, Q. Zhang, J. Dang, C. Yin, and S. Chen, "Preparation and properties of polystyrene/SiCw/SiCp thermal conductivity composites," *Journal of Applied Polymer Science*, vol. 124, no. 1, pp. 132–137, 2012.
- [30] A. J. Knowles, X. Jiang, M. Galano, and F. Audebert, "Microstructure and mechanical properties of 6061 Al alloy based composites with SiC nanoparticles," *Journal of Alloys and Compounds*, vol. 615, pp. S401–S405, 2014.
- [31] C. Fenghong, C. Chang, W. Zhenyu, T. Muthuramalingam, and G. Anbuhezhiyan, "Effects of silicon carbide and tungsten carbide in aluminium metal matrix composites," *Silicon*, vol. 11, no. 6, pp. 2625–2632, 2019.
- [32] S. V. Nair, J. K. Tien, and R. C. Bates, "SiC-reinforced aluminium metal matrix composites," *International Metals Reviews*, vol. 30, no. 1, pp. 275–290, 1985.
- [33] E. Gikunoo, O. Omotoso, and I. N. A. Oguocha, "Effect of fly ash particles on the mechanical properties of aluminium casting alloy A535," *Materials Science and Technology*, vol. 21, no. 2, pp. 143–152, 2005.
- [34] V. Aggarwal, C. I. Pruncu, J. Singh, S. Sharma, and D. Y. Pimenov, "Empirical investigations during WEDM of Ni-27Cu-3.15Al-2Fe-1.5Mn based s for high temperature corrosion resistance applications," *Materials*, vol. 13, no. 16, p. 3470, 2020.
- [35] D. Doreswamy and J. Javeri, "Effect of process parameters in electric discharge machining of D2 steel and estimation of coefficient for predicting surface roughness," *International Journal of Machining and Machinability of Materials*, vol. 20, no. 2, pp. 101–117, 2018.
- [36] D. Deepak, P. Shrinivas, G. Hemant, and R. Iasy, "Optimization of current and pulse duration in electric discharge drilling of D2 steel using graphite electrode," *International Journal of Automotive and Mechanical Engineering*, vol. 15, no. 4, pp. 5914–5926, 2018.